Grid Convergence Study for Detached-Eddy Simulation of Flow over Rod-Airfoil Configuration Using OpenFOAM

IOP Conf. Series: Materials Science and Engineering **491** (2019) 012023 doi:10.1088/1757-899X/491/1/012023

Grid Convergence Study for Detached-Eddy Simulation of Flow over Rod-Airfoil Configuration Using OpenFOAM

Siti Ruhliah Lizarose Samion[1, a], Nur Haziqah Shaharuddin[1, b] and Mohamed Sukri Mat Ali[1, c]

[1]Malaysia-Japan International Institute of Technology, University of Technology Malaysia, 54100 Kuala Lumpur, Malaysia

E-mail: [a]lializarose@gmail.com; [b]haziqahshaharuddin11@gmail.com; [c]researchsukri@gmail.com

Abstract. A rod-airfoil is a benchmark configuration for simulating Airfoil-Turbulence Interaction Noise (ATIN). The numerical simulation is modelled using unsteady Detached Eddy Simulation (DES). The grid refinement involves two stages of assessments. The first compares the sensitivity of two reasonable estimated cells to the flow behaviours of the case. Based on the finding from the first stage, further grid refinement is proceed in stage two. In stage two, a minimum of three different grid resolutions are considered; the fine, medium and coarse grids in order to investigate the grid independency. Richardson extrapolation and Grid Convergence Index (GCI) are introduced to quantitatively evaluate the grid independency. Based on the results between those three different grids, a monotonic convergence criterion has been achieved. The reduction in GCI value indicates that the grid convergence error has been significantly reduced, in which the fine grid has a GCI value is around less than 0.5%.

1. Introduction

An airfoil is a common engineering geometry. Its application especially in the wind turbines, turbofan engines and the helicopter rotors, however induces generation of airfoil- turbulence interaction noise (ATIN) [1,2,3]. The airfoil experiences undulation of lift as a result of unsteady pressure fluctuations produced by the interaction of turbulence in the upstream flow and the airfoil leading edge, and consequently it is responsible for the ATIN [4]. The ATIN is mostly noticeable at lower frequency because larger turbulent structures are the strongest in its noise generation mechanism [5].

The turbulence physics upstream of airfoil is an important feature in the ATIN study as it governs the noise generating mechanism. Thus, ATIN reduction should be correlated with the upstream turbulent characters. However, the correlation is not yet been discussed comprehensively I the open literature.

In most ATIN investigations, the upstream turbulence is generated and conveyed downstream to the airfoil by vortex generator so that the same condition of ATIN can be mimicked as in real condition[6, 7, 8]. Extensions of unsteady CFD techniques to the prediction of ATIN generated by high Reynolds number flows in complex geometries have first to be benchmarked on relevant test cases. Such a test case must be based on geometry that contains some of the aerodynamic mechanisms encountered in ATIN applications, but remain simple enough from the computational point of view in order to achieve parametric study purposes. The rod-airfoil configuration is a relevant benchmark case

for the ATIN investigation. Jacob et al [9] was among the pioneer to introduce this rod-airfoil configuration. This is because at high Reynolds numbers, the rod sheds the well-known von Karman vortex street which acts as an oncoming disturbance onto the airfoil. Jacob et al. [9] highlighted three strong dimensional effects responsible for spectral broadening around the rod vortex shedding frequency in the subcritical regime, and identified that the airfoil leading edge was the main contributor to the noise emission in a rod-airfoil configuration due to vortex-structure interaction. Moreover, further understanding on the details of the rod-airfoil interactions have been gained through numerical simulations too. Previous studies [10,11,12,13,14,15] found good agreement between numerical calculation and experiment of ATIN. Hence, the current study aims to provide a systematic approach for grid convergence study of flow around a rod-airfoil using Grid Convergence Index (GCI) that is based on Richardson extrapolation.

2. Numerical model description

2.1 Test case and mesh description

The investigated case is a rod-airfoil configuration in a three-dimensional uniform incompressible flow at constant free stream velocity. The test case is as illustrated in Figure 1. A rod with diameter D with a downstream airfoil of chord length $9.5D$ immersed in a fluid of constant free stream velocity U_∞. The geometrical parameters and flow dynamic quantities are non-dimensionalized by D and U_∞ respectively. Gap distance between the rod and airfoil is set $3.5D$ as according to Yong Li et al. [16] the airfoil will experience fully developed vortex in the rod wake. The upstream, downstream, up and bottom boundary distance are also mentioned in the schematic diagram of computational domain. The span distances are $10D$ for the early stage grid refinement and $3.5D$ in the later.

The grid convergence performance was assessed by two stages. Table 1 presents the number of grid for different cases investigated in current study.

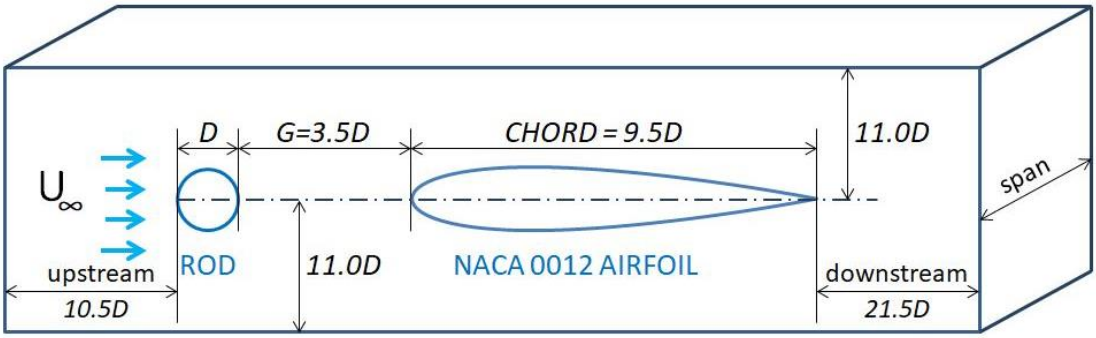

Figure 1. Model configuration in the simulation domain with the parameters. (Figure not in scale.)

Table 1. Number of grids of different cases.

Grid Refinement Stage	CASE	$N_x \times N_y \times N_z$
Stage 1 (span$10D$)	A	17,040
	B	180,680
Stage 2 (span $3.5D$)	C	1,042,720
	D	1,783,740
	E	3,153,200

2.2 Solution Methodology

The rod-airfoil study involves turbulence structure investigation because it was primarily aimed to investigate the noise emission. The most effective simulation model to incorporate fairly well with

turbulence is the Large Eddy Simulation (LES) if compared to the Reynolds Average Navier-Stokes (RANS). However, current study implemented Detached Eddy Simulation (DES) computations on the flow over the rod-airfoil due to the high demand of computational cost of the LES. All flow conditions and settings are summarized in Table 2.

Table 2. Flow conditions and setting.

Reynolds Number, $\mathrm{Re} = \frac{\mathrm{U}_\infty D}{\nu}$	20,000
Mach Number, Ma	0.044
Turbulent Model	Spallart-Allmaras DDES
Time step, Δt (s)	$1.5 \sim 2.0\times 10^{-4}$

Computations in this work were performed using OpenFOAM. In particular, the merged piso-simple algorithm known as pimpleFoam solver is used. The convergence criterion for pressure and velocity solutions is set so the residuals fall below the tolerance of 10^{-9} and 10^{-8} respectively at each time step. 2nd order backward scheme is used for the temporal discretisation. The convection term is discretized using Gauss linearUpwind grad (U) and the viscous term is discretized using Gauss Gamma scheme. The time step is set accordingly as to keep the CFL value less than unity.

3. Grid Refinement Stage 1

Firstly at this stage, two cases are compared to obtain the grid refinement reliability. Two cases were prepared – one with the coarsest grids with smallest cell height as $\boldsymbol{0.2D}$ and the other is with smallest cell height approximately $\boldsymbol{0.05D}$. The visualisation of flow and the $\boldsymbol{y^+}$ values are assessed at this stage from each case**.**

3.1 Flow visualisation

Figure 2 depicts the grid distribution of the case with the $\boldsymbol{y^+}$ values of the geometry. The wall $\boldsymbol{y^+}$ is a non-dimensional wall distance often used in CFD defining the ratio between turbulent and laminar influences in a cell. Near-wall regions have bigger gradients in variables and in the flow physical momentum. The simulation adopts wall function in the calculation thus the $\boldsymbol{y^+}$ values are bound to meet in the range of $\boldsymbol{30 \leq y^+ \leq 60}$ [17]. Values of $\boldsymbol{y^+ \approx 30}$ are most desirable for wall functions [18]. Hence, based on the $\boldsymbol{y^+}$ values comparison, the grids of case B is more preferable due to the rod's $\boldsymbol{y^+}$ value is nearer to 30**.**

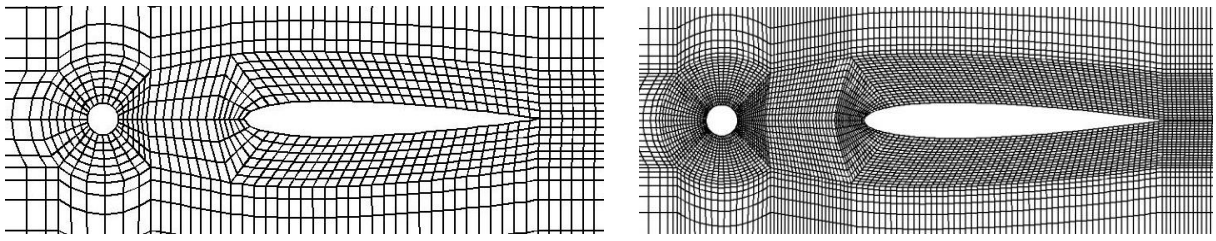

(a) Case A with $y^+_{\mathrm{rod}} \approx 60$ and $y^+_{\mathrm{airfoil}} \approx 38$ (b) Case B with $y^+_{\mathrm{rod}} \approx 41$ and $y^+_{\mathrm{airfoil}} \approx 32$.

Figure 2. Cell distribution around the rod-airfoil.

The flow visualization is then assessed in Figure 3. Flow separations are observed in both cases. However, the shear layers formation is not visible in case A. This instantaneous streamwise velocity results of case A shows not-properly formed vortex shedding if compared to that of Case B's. The alternation of the shear layers in the downstream of the rod is clear in Case B. This proves the fine grids reliability in Case B is able to reproduce the expected vortex shedding.

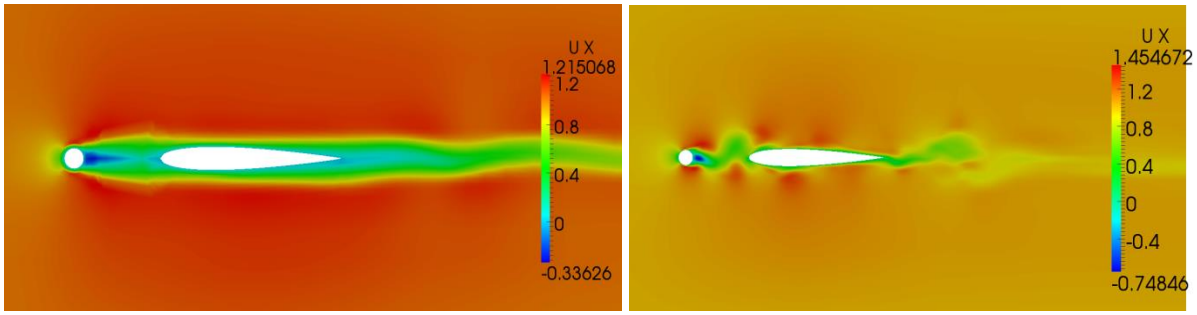

Figure 3. Instantaneous streamwise velocity contours at $z = 0$. LHS: Case A. RHS: Case B.

The flow visualization of the spanwise plane right upstream ($0.5D$ in front) from the airfoil is also compared as shown in Figure 4. The flow behaviour in spanwise direction is useful for inspection of spanwise correlation length.

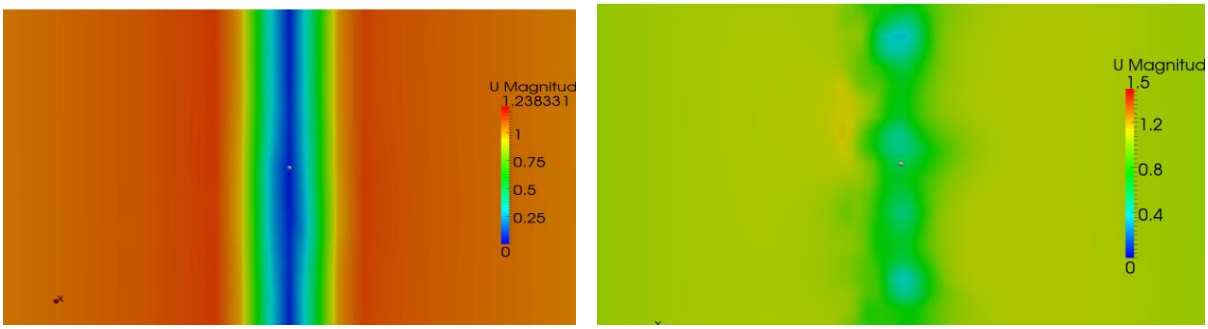

Figure 4. Instantaneous streamwise velocity contours crossectional at $= -0.5D$.
LHS: Case A. RHS: Case B.

4. Grid Refinement Stage 2

Three different grid resolutions were used in this stage. The coarsest is Case C, case D has medium grid and the finest is Case E. The upstream , top and bottom is $10D$ away from the boundary, while the outlet is $20D$ away from the boundary and the span length is $3.5D$.

4.1 Grid convergence study by Richardson extrapolation

Richardson extrapolation, introduced by Richardson [19] is also known as "the differed approach to the limit $(h \to 0)$". It defines a higher-order estimate of flow fields from a series of lower-order discrete values $(f_1, f_2, , , , , f_n)$. A convergence study needs three grid resolutions at minimum [20]. Roache [21] has generalized Richardson Extrapolation by introducing the p^{th}order methods:

$$f_{exact} \approx f_1 + |(f_1 - f_2)/|(r^p - 1)| \quad (1)$$

The grid refinement ratio r in this study is fixed, and defined as $r = \Delta_C/\Delta_D = \Delta_D/\Delta_E = 1.7$

From equation (1), the extrapolated value is varied by p^{th}order decision. As stated in Stern [19], the order of accuracy can be estimated by using the following equation:

$$p = \frac{ln(\varepsilon_{32}/\varepsilon_{21})}{ln(r)} \quad (2)$$

$$\varepsilon_{i+1,i} = f_{i+1} - f_i \quad (3)$$

To evaluate the extrapolated value from these solutions, the convergence of the system must be first determined. The possible convergence conditions are: (1) Monotonic convergence : 0 < R < 1 (2) Oscillatory convergence : R < 0 and (3) Divergence : R > 1, where R is the convergence ratio and it is determined by the R = ε_{32} / ε_{21} .

Table 3 summarizes the order of accuracy for root mean square lift coefficient CL_{rms} and mean drag coefficient CD_{mean} from the simulation results of the three different grids. The convergence is monotonic for both variables assessed. Strouhal number St results are not included in this analysis due to the differences between all the cases are not significantly big.

Table 3. Order of accuracy Grid Convergence Index for the flow variables.

	ε_{32}	ε_{21}	R	p	GCI_{32} (%)	GCI_{21}(%)
CL_{rms}	0.1091	0.0076	0.0696	4.6763	4.71	0.34
CD_{mean}	0.1515	0.0015	0.0099	8.1008	0.25	0.0024

The Grid Convergence Index (GCI) defines a uniform measure of convergence for grid refinement studies as stated in Roache [21]. The GCI is derived from estimated fractional error obtained from the generalization of Richardson extrapolation. The GCI value represents the resolution level and how much the solution approaches the asymptotic value. The GCI for thefine grid resolutions can be calculated by the following:

$$GCI_{i+1,i} = F_s \frac{|\varepsilon_{i+1,i}|}{f_i(r^p-1)} \tag{4}$$

The safety factor F_s selected for the study is 1.25 as followed from Wilcox [22]. As observed from Table 3 previously, there is reduction in GCI values for the three successive grids ($GCI_{21} < GCI_{32}$). The GCI for finer grid GCI_{21} is relatively low compared to the GCI of the coarser one GCI_{32}. This implies that the dependency of the numerical simulation on the cell size has been reduced. In addition, the grid independent solution is acceptably achieved due to the GCI reduction from coarser grid to the finer grid. In other words, further refinement will not result in much change.

The variables obtained are compared with the extrapolated value using Equation (1). The comparisons are then plotted in Figure 4. The extrapolated value of CL_{rms} is just slightly lower than that of finer grid results (h/D=0.001D). Therefore, it is proved that the solution is converged within the refinement from coarser to the finer grid. Also, in this paper the discrepancy between the simulation value and this extrapolated value is defined as the error

$$E_i = \frac{f_i - f_{RE}}{f_{RE}} \tag{5}$$

Figure 5 shows that the successive grid refinement has nearly achieved the asymptotic value at the finest grid resolution where the relative error compared with the RE is only 0.002%, hence it is grid independent.

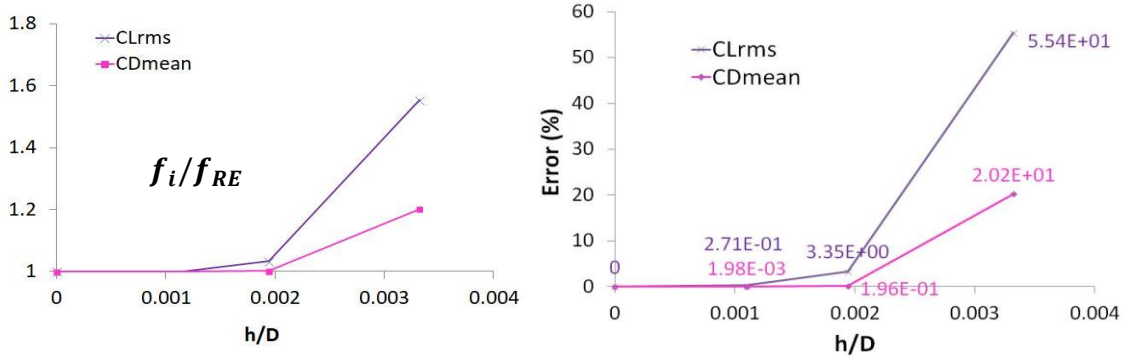

Figure 5. LHS: Comparison of global parameters normalized by the extrapolated value, among the three grid solutions. Extrapolated values are based on Richardson Extrapolation estimation. RHS: Error percentage for the global parameters of rod.

4.2 *Results comparison with previous studies*

Table 4 compares the results of current DES with previous studies of the same case. The Strouhal number is in excellent agreement with the literature. The root mean square lift coefficient and mean drag coefficient are slightly lower, but they are still in good agreement.

Table 4. Comparison of global flow dynamic quantities with previous literature.

Cases	Year	Reynolds number	Method	$CL_{\mathbf{rms}}$	$CD_{\mathbf{mean}}$	St
Cantwell & Coles	1983	140,000	Exp. (rod only)	0.3-0.4	1.0-1.35	0.19
Casalino et al.	2003	49,000	URANS	-	0.8	0.24
Greschner et al.	2008	48,000	k-ε DES	0.42	0.81	0.185
Giret et al.	2015	48,000	LES	0.41	0.92	0.2
Current study (case E)	**2018**	**20,000**	**DES**	**0.209**	**0.756**	**0.19**

5. Conclusion

Two stages of grid assessments were carried out in this paper to obtain the best grid suitable for a rod-airfoil simulation in a Detached Eddy Simulation (DES) model at high Reynolds number flow. The first stage has obtained the grid with better flow visualization that captures a well developed vortex shedding in the wake of rod and airfoil. However, this result is the early onset to a further grid refinement assessment in the next stage.

The next stage of grid refinement has provided good insights on the grid independency of especially the finest grid proposed. The GCI inspection of the flow variables showed that there was a gradual reduction when the grid system was refined. Also, the when the extrapolated value from Richardson Extrapolation are compared with current results, the results of finer grid (case E) showed good performance. Hence, the grid from case E is appropriate to be used further in the next analysis of rod airfoil due to the GCI values are all less than 0.5%.

Acknowledgments

The authors would like to wish and acknowledge University of Technology Malaysia for the grantment of Ainuddin Wahid Scholarship that has support this study financially.

References

[1] Amiet, RK. 1975 Acoustic radiation from an airfoil in a turbulent stream. *J. Sound and Vib.* **41** 407-420
[2] Arbey, H and Bataille, J. 1983 Noise generated by airfoil profiles placed in a uniform flow. *J. Fluid Mech.* **134** 33-47
[3] Paterson, RW. and Amiet, RK. 1976 Acoustic radiation and surface pressure characteristics of an airfoil due to incidence turbulence. NASA CR-2733
[4] Blake, W.K. 1986 Mechanics of Flow-induced Sound and Vibration. 2 *Vols. Academic Press.* New York
[5] Oerleman, S. and Migliore, P. 2004 Aeroacoustic Wind Tunnel Tests of Wind Turbine Airfoils. *National Aerospace Laboratory NLR*, Emmeloord, The Netherlands 319
[6] Jackson, R., Graham, JMR. and Maull. DJ. The lit on a wing in a turbulent flow. *Aeronautical Quarterly*
[7] Jurdic, V. 2005 Effect of an angle of attack and airfoil shape on turbulence-interaction noise. *AIAA/CEAS Aeroacoustic Conference Meeting and Exhibit*, 22-25 May
[8] Bachmann, T., Klan. S., Baumgartner, W., Klaas, M., Schroder, W. and Wagner, H. 2007 Morphometric characterization of wing feathers of the barn owl Tyto alba pratincola and pigeon Columbia livia, *Front Zoo* **4** 1-15.
[9] Jacob, MC., Boudet, J., Casalino, D., and Michard, M. 2005 A rod-airfol experiment as benchmark for broadband noise modelling. Theorotical and Computational Fluid Dynamics. **10** 171-196

[10] Casalino, D., JHacob, M. and Roger, M. 2003 Prediction of Rod-Airfoil Interaction Noise using Ffowccs-William Hawkings Analogy. *AIAA Journal*. **41** 2.
[11] Sorguven, E., Magagnato, F., and Gabi, M. 2003 Acoustic prediction of a cylinder and airfoil configuration at high Reynolds numbers with LES and FWH. *ERCOFTAC* Bulletic **58** 47-50.
[12] Boudet, J., Grosjan, N. and Jacob, M. 2005 Wake-airfoil interactions as broadbandnoise source: A large eddy simulation study. *International Journal of Aeroacoustic* 4 **1** 93-115.
[13] Magaganato, F., Sorguven, E. and Gabi, M. 2003 Far-field noise prediction by large eddy simulation and Ffowccs-Williams and Hawkings Analogy. *AIAA* 3206
[14] Grecshner, B., Thiele, F., Jacob, M. and Casalino, D. 2008 Prediction of sound generated by a rod- airfoil configuration using EASMDES and the generalized Lighthill/FWH Analogy. *Computers and Fluids* 37 **4** 402-413.
[15] Berland, J., Lafon, P., Crouzet, F., Daude, F. and Baily, C. 2010 Numerical insight into sound sources of a rod-airfoil flow configuration using direct noise calculation. *AIAA* 3705
[16] Yong Li, Wang, X., Chen, Z. and Li, Z., 2014 Experimental study of vortex-structure interaction noise radiated from rod-airfoil configurations. *Journal of Fluids and Structures*. **51** 313-325
[17] Fluent 6.2, 2006 Documentation File, ANSYS Manual
[18] Salim M. Salim and Cheah SC. March 18-20 2009 Wall y+ strategy for dealing with wall-bounded turbulent flows. *Proceedings of Int. Multiconference of Engineers and Computer Scientists*. **2**
[19] Richardson, LF and Gaunt JA, 1927. The deferred approach to the limit. Part I. Single lattice. Part II. Interpenetrating lattices, *Philosophical Transactions of the Royal Society of London. Series A. Containing Papers of A Mathematical or Physical Character*. **226** 299-361
[20] Stern, F., Wilson, RV, Coleman, WH. And Patterson EG , .2001. Comprehensive approach to verification and validation of CFD simulations Part I. Methodology and Procedures. *Journal of Fluids Engineering* 123 **4** 793-802
[21] Roache, PJ. 1994. Perspective: A method for uniform reporting of grid refinement studies. *Journal of Fluid Engineering*. 116 **3** 405-411
[22] Wilcox, DC. 2006. The effect of circular cylinders between crossflow. *Journal of Fluids and Structures*. 1 **2** 239-261